Biophysical Journal, Volume 97

Supporting Material

1D mathematical model of the atrioventricular node including AN, N and NH cells

Shin Inada, Jules C. Hancox, Henggui Zhang, and Mark R. Boyett

DATA SUPPLEMENT

1D mathematical model of the atrioventricular node including AN, N and NH cells

S. Inada, J.C. Hancox, H. Zhang and M.R. Boyett

Methods

A glossary of terms is given in Table S1.

Models of AN, N and NH action potentials

Models were developed for the rabbit, because of the relative plethora of experimental data for this species. Hodgkin-Huxley type models were developed, because there are insufficient experimental data for the development of Markov-type models. The models are a nonlinear dynamic system of 26 simultaneous ordinary differential equations.

Cell capacitance

Munk *et al.*(1) showed that the cell capacitance (C_m) of rod-shaped atrioventricular node (AVN) cells with an AN-like action potential configuration is larger (~41 pF) than that of ovoid AVN cells with N- or NH-like action potential configurations (~29 pF). Ren *et al.* (2) reported that the C_m of AN, N and NH cells to be ~49, ~26 and ~35 pF, respectively. We assumed C_m to be 40 pF for AN and NH cells and 29 pF for an N cell.

Ionic currents

As shown in Table S2, membrane potential was calculated from the sum of ten ionic currents: Na^+ current (I_{Na}), L-type Ca^{2+} current ($I_{Ca,L}$), transient outward K^+ current (I_{to}), rapid delayed rectifier K^+ current ($I_{K,r}$), hyperpolarization-activated current (I_f), sustained inward current (I_{st}), inward rectifier K^+ current ($I_{K,1}$), Na^+-Ca^{2+} exchange current (I_{NaCa}), Na^+-K^+ pump current (I_p) and background current (I_b).

$\boldsymbol{I_{Na}}$**.** The formulation for I_{Na} was taken from the model of the rabbit atrial action potential of Lindblad *et al.* (3). I_{Na} is a large fast inward current responsible for the rapid upstroke of the action potential in atrial and ventricular muscle - the maximum upstroke velocity (dV/dt_{max}) of rabbit atrial muscle is ~150 V/s (4). In contrast to atrial muscle, dV/dt_{max} of the AVN is low: ~45 V/s in the AN region, ~13 V/s in the N region and ~30 V/s in the NH region in the rabbit (Fig. 2). Consistent with this, Munk *et al.* (1) and Ren *et al.* (2) showed that, in the rabbit, I_{Na} is absent in putative N cells, but present in putative AN and NH cells. In addition, in the rabbit, whereas Na^+ channel mRNA and protein are present in the atrial muscle, they are absent or expressed at a greatly reduced level in the inferior nodal extension (mRNA) (5) and the midnodal cells of the proximal penetrating bundle (protein) (6), both regions where N cells are assumed to be located. In this study, it was assumed that I_{Na} is present in the AN and NH regions, but not in the N region — in the AN and NH regions, the conductance was chosen to give an appropriate dV/dt_{max}. Equations for I_{Na} are given in Table S3.

$\boldsymbol{I_{Ca,L}}$**.** A new formulation was developed for $I_{Ca,L}$ based on voltage clamp data from rabbit AVN cells. For $I_{Ca,L}$, Fig. S1 shows activation and inactivation curves, time constants of inactivation, current-voltage relationships, recovery from inactivation, and the current profile during a voltage clamp pulse. Recovery from inactivation includes both fast and slow components (Table S4, equations 6-10). In Fig. S1, symbols show experimental data and smooth lines show model data. The model data are a reasonable fit to the experimental data. In the rabbit, mRNA for Ca_v1 channel subunits (responsible for $I_{Ca,L}$) is present throughout the rabbit AVN as well as the atrial muscle (5). The N region shows pacemaking and, in order for the take-off potential of the model action potential to match that recorded in experiments, the activation curve had to be shifted to more negative potentials. Perhaps consistent with this, whereas $Ca_v1.2$ mRNA is present in the working myocardium, $Ca_v1.3$ mRNA is present in the AVN (as it is in the SAN); $Ca_v1.3$ has a more negative activation threshold than $Ca_v1.2$ (5). The conductance was chosen to give a current density (−12.3, −12.9 and −13.9 pA/pF in AN, N and NH cells, respectively; measured during pulse to 0 mV from holding potential of −40 mV) close to that measured experimentally (−3.3 to −16.4 pA/pF (7-13);

measured during pulse to 0 or +5 mV from holding potential of −40 mV). The conductance was also chosen to give the best shape and duration of the computed action potential (as compared to experimentally recorded action potentials) in terms of upstroke velocity, action potential amplitude, height and duration of the plateau phase, and overall action potential duration. Equations for $I_{Ca,L}$ are given in Table S4.

***I_{to}*.** A new formulation was developed for I_{to} based on voltage clamp data from rabbit AVN cells. For I_{to}, Fig. S2 shows activation and inactivation curves, time constants of inactivation, the current profile during voltage clamp pulses, the current-voltage relationship, and recovery from inactivation - symbols show experimental data and smooth lines show model data. The model data are a reasonable fit to the experimental data. Munk *et al.* (1) reported that there is I_{to} in 93 % of putative AN cells and only 42 % of putative N and NH cells. Perhaps consistent with this, in the rabbit, whereas mRNAs for $K_v1.4$ and KChIP2 (two ion channel subunits responsible for I_{to}) are abundant in the working myocardium, they are absent from the inferior nodal extension (assumed to be made up of N cells) (5). In this study, it was assumed that I_{to} is present in the AN and NH regions - the conductance was chosen to give a current density (49.6 and 34.7 pA/pF in AN and NH cells, respectively; measured during pulse to +40 mV from holding potential of −80 mV) close to that measured experimentally (42.9 pA/pF (14); measured during pulse to +40 mV from holding potential of −80 mV). It was assumed that I_{to} is absent in the N region. Equations for I_{to} are given in Table S5.

***$I_{K,r}$*.** $I_{K,r}$ has been recorded in rabbit AVN cells (15, 16). Although $I_{K,s}$ (slow delayed rectifier K^+ current), as well as $I_{K,r}$, has been identified in the rabbit SAN (17), $I_{K,s}$ has been reported to be absent from the rabbit AVN and only $I_{K,r}$ is present (15, 18). In the rabbit, ERG mRNA (responsible for $I_{K,r}$) is perhaps 20× more abundant than K_vLQT1 and minK mRNAs (responsible for $I_{K,s}$) in the AVN (5). In this study, it was assumed that only $I_{K,r}$ is present in the AVN. A new formulation was developed for $I_{K,r}$ based on voltage clamp data from rabbit AVN cells. For $I_{K,r}$, Fig. S3 shows the activation curve, time constants of activation, current-voltage relationships, and the current profile during voltage clamp pulses - symbols show experimental data and smooth lines show model data. The model data are a reasonable fit to the experimental data. The conductance for $I_{K,r}$ was chosen to give a current density (0.5, 1.7 and 0.7 pA/pF in AN, N and NH cells, respectively; measured at end of 500 ms pulse to +20 mV from holding potential of −40 mV) close to that measured experimentally (0.7 and 1.1 pA/pF (16); measured at end of 500 ms pulse to +10 or +30 mV, respectively) and an appropriate action potential duration. Equations for $I_{K,r}$ are given in Table S6.

***I_f*.** A new formulation was developed for I_f based on voltage clamp data from rabbit AVN cells. For I_f, Fig. S4 shows the activation curve, time constants of activation, the current-voltage relationship, and the current profile during voltage clamp pulses - symbols show experimental data and smooth lines show model data. The model data are a reasonable fit to the experimental data. Munk *et al.* (1) showed that the magnitude of I_f at -100 mV in putative N and NH cells is 25 times that in putative AN cells. Furthermore, Munk *et al.* (1) reported that the activation range for I_f in putative N and NH cells is more positive than that for putative AN cells. HCN4 is the principal ion channel subunit responsible for I_f and, consistent with the electrophysiology, HCN4 mRNA and protein are abundant throughout the inferior nodal extension (assumed to be made up of N cells) in the rabbit (5, 19); HCN4 mRNA, at least, is absent from the transitional region (assumed to be made up of AN cells) and only weakly abundant in the penetrating bundle (assumed to be made up of NH cells). In this study, it was assumed that I_f is only present in the N region - the conductance was chosen to give a current density (−1.8 pA/pF; measured during 2 s pulse to −100 mV from holding potential of -40 mV) close to that measured experimentally (−1.7 to −2.0 pA/pF (1, 20, 21); measured during 1 or 2 s pulse to ~−100 mV from holding potential of −40 or −50 mV). Equations for I_f are given in Table S7.

***I_{st}*.** In the rabbit AVN, Guo and Noma (10) reported a novel current, I_{st}. I_{st} was included in the model and the description of the current is based on the voltage clamp data of Guo and Noma (10). The formulation for I_{st} was taken from Guo and Noma (10) and the model of the rabbit SAN action potential of Kurata *et al.* (22). The activation curve, recordings of I_{st} during depolarizing voltage-clamp pulses and the current-voltage relationship are shown in Fig. S5. The activation curve was calculated from published experimental data. I_{st} was assumed to be significant in N cells, but not in AN cells, to give appropriate action potential shapes. Equations for I_{st} are given in Table S8.

$\boldsymbol{I_{K,1}}$**.** The formulation $I_{K,1}$ was taken from the model of the rabbit atrial action potential of Lindblad *et al.* (3). $I_{K,1}$ is responsible for the resting potential in the working myocardium. An $I_{K,1}$-like current occurs at negative potentials in guinea-pig AVN cells. However, $I_{K,1}$ has been reported to be small or absent in rabbit AVN cells (1, 23, 24). $K_{ir}2$ channels are responsible for $I_{K,1}$. In the mouse, there is evidence that $K_{ir}2.1$ is absent in the penetrating bundle (which possibly contains some N cells at least), but is present in surrounding cells (some of which may be AN cells) (25). In this study, it was assumed that $I_{K,1}$ is absent from N cells. However, it was assumed that some $I_{K,1}$ is present in AN and NH cells - it was required to reproduce the more negative maximum diastolic potential (MDP) and the greater dV/dt_{max} of both AN and NH cells (as compared to those of the N cell). Equations for $I_{K,1}$ are given in Table S9.

$\boldsymbol{I_{NaCa}}$**,** $\boldsymbol{I_{p}}$ **and** $\boldsymbol{I_{b}}$**.** Both I_{NaCa} and I_p have been demonstrated in rabbit AVN cells (26, 27) and mRNAs for NCX1 (responsible for Na^+-Ca^{2+} exchanger) and the α1 isoform of the Na^+-K^+ pump are present in the rabbit AVN (1, 5). The formulation for I_{NaCa} was taken from the model of the rabbit SAN action potential of Kurata *et al.* (22), and the formulation for I_p was taken from the model of the rabbit SAN action potential of Zhang *et al.* (28). The density of I_{NaCa} is similar to that in experiments on rabbit AVN cells (22, 28) as shown in Fig. S6. Equations for I_{NaCa} and I_p are given in Tables S10 and S11. The model includes a background current, I_b. The conductance and equilibrium potential of I_b was adjusted to obtain a reasonable resting potential. The equation for I_b is given in Table S11.

Intracellular ionic concentrations

For simplicity, intracellular Na^+ and K^+ concentrations in AN, N and NH cells were assumed to be constant (8 mM and 140 mM, respectively). Intracellular Ca^{2+} affects nodal tissues (29). The intracellular Ca^{2+} concentration was either assumed to be constant (10^{-7} M; as in our model of rabbit SAN cells (28)) or, alternatively, intracellular Ca^{2+}-handling was modelled using a system of equations based on the model developed by Kurata *et al.* (22) for rabbit SAN cells (Table S12). Calculated Ca^{2+} transients are shown in Fig. S6. The results obtained with the two strategies (with and without intracellular Ca^{2+}-handling) were qualitatively similar; only data obtained using the models incorporating intracellular Ca^{2+}-handling are shown here.

Via the Na^+-Ca^{2+} exchanger, intracellular Ca^{2+} is expected to affect electrical activity. When either Na^+-Ca^{2+} exchange was blocked or intracellular Ca^{2+} was kept constant (fixed to 10^{-7} M), there was a shortening of the action potential (in AN and NH cells at least) and a slowing of pacemaking (in the N cell) (data not shown). We have observed a similar shortening of the action potential in ventricle on buffering intracellular Ca^{2+} (30) and a slowing of pacemaking in the AV node when the intracellular Ca^{2+} transient is abolished by the application of ryanodine (31).

One-dimensional (1D) multicellular model

A simplified 1D multicellular model (string of cells) for the SAN, right atrium and AVN of the rabbit was developed. The string of cells representing the SAN included both small central and large peripheral cells. Action potentials in rabbit central and peripheral SAN cells were calculated using the model of Zhang *et al.* (28). In the Zhang *et al.* (28) model, central cells have a C_m of 20 pF and peripheral cells have a C_m of 65 pF and ionic current densities are a function of C_m. Within the string of SAN cells, C_m (and thus cell type) was increased from the centre to the periphery as described in Table S13 (equation 1). The action potential in rabbit atrial cells was calculated using a modified version of the model of Lindblad *et al.* (3). Action potentials in rabbit AN, N and NH cells were calculated using the models described above. Neighbouring cells were coupled by a coupling conductance, g_j. The coupling conductance was varied to give appropriate conduction times and velocities.

At the border of atrial muscle and nodal cells, the coupling conductance, g_j, was changed in a gradient fashion as described by equations 8 and 9 in Table S13, and equations 6 and 7 in Table S14. In addition, at the border of the atrial muscle with NH cells, the Na^+ conductance, g_{Na} (governing I_{Na}), was changed in a gradient fashion as described by equations 13 and 15 in Table S13, and equations 10 and 12 in Table S14. The gradients in coupling conductance and Na^+ channel conductance were not necessary for normal conduction through the AVN. However, reentry was sensitive to the gradients. For example, in the model shown in Fig. 5A, when the gradients were removed, reentry did not occur.

We used non-flux boundary conditions for both ends of the string of cells

Computational methods

All constants and starting values are listed in Tables S15-S18. Table S17 also shows the differences between the original and modified (as used in simulations) versions of the Lindblad *et al.* (3) model of the rabbit atrial action potential. The intracellular K^+ concentration was also different: whereas in the original model it is 100 mM, in the modified version it is ~140 mM (Table S18). The simultaneous nonlinear ordinary differential equations were solved numerically. The models were coded in the C++ language and run on a personal computer with the UNIX operating system and a workstation with the Linux operating system. A Runge-Kutta-Fehlberg numerical integration method (RKF45) was used to solve the ordinary differential equations. A time step of 5 μs was used; this gives a stable solution of the equations and maintains the accuracy of the computation of membrane current and potential (32). The codes for the atrial, AN, N and NH cell models are available as part of the Data Supplement.

REFERENCES

1. Munk, A. A., R. A. Adjemian, J. Zhao, A. Ogbaghebriel, and A. Shrier. 1996. Electrophysiological properties of morphologically distinct cells isolated from the rabbit atrioventricular node. *J. Physiol*. 493:801-818.
2. Ren, F. X., X. L. Niu, Y. Ou, Z. H. Han, F. D. Ling, S. S. Zhou, and Y. J. Li. 2006. Morphological and electrophysiological properties of single myocardial cells from Koch triangle of rabbit heart. *Chin. Med. J.* 119:2075-2084.
3. Lindblad, D. S., C. R. Murphey, J. W. Clark, and W. R. Giles. 1996. A model of the action potential and underlying membrane currents in a rabbit atrial cell. *Am. J. Physiol*. 271:H1666-H1696.
4. Yamashita, T., T. Nakajima, H. Hazama, E. Hamada, Y. Murakawa, K. Sawada, and M. Omata. 1995. Regional differences in transient outward current density and inhomogeneities of repolarization in rabbit right atrium. *Circulation*. 92:3061-3069.
5. Greener, I. D., J. O. Tellez, H. Dobrzynski, M. Yamamoto, R. Billeter-Clark, and M. R. Boyett. 2006. Distribution of ion channel transctipts in the rabbit atrioventricular node as studied using in situ hybridisation and quantitative PCR. *J. Mol. Cell. Cardiol*. 40:982-983.
6. Petrecca, K., F. Amellal, D. W. Laird, S. A. Cohen, and A. Shrier. 1997. Sodium channel distribution within the rabbit atrioventricular node as analysed by confocal microscopy. *J. Physiol*. 501:263-274.
7. Nakayama, T. and H. Irisawa. 1985. Transient outward current carried by potassium and sodium in quiescent atrioventricular node cells of rabbits. *Circ. Res.* 57:65-73.

8. Hancox, J. C. and A. J. Levi. 1994. L-type calcium current in rod- and spindle-shaped myocytes isolated from rabbit atrioventricular node. *Am. J. Physiol*. 267:H1670-H1680.
9. Wang, D., J. C. Shryock, and L. Belardinelli. 1996. Cellular basis for the negative dromotropic effect of adenosine on rabbit single atrioventricular nodal cells. *Circ. Res.* 78:697-706.
10. Guo, J. and A. Noma. 1997. Existence of a low-threshold and sustained inward current in rabbit atrio-ventricular node cells. *Jpn. J. Physiol*. 47:355-359.
11. Hancox, J. C. and J. S. Mitcheson. 1997. Inhibition of L-type calcium current by propafenone in single myocytes isolated from the rabbit atrioventricular node. *Br. J. Pharmacol.* 121:7-14.
12. Mitcheson, J. S. and J. C. Hancox. 1997. Modulation by mexiletine of action potentials, L-type Ca current and delayed rectifier K current recorded from isolated rabbit atrioventricular nodal myocytes. *Pflügers Arch.* 434:855-858.
13. Sato, N., H. Tanaka, Y. Habuchi, and W. R. Giles. 2000. Electrophysiological effects of ibutilide on the delayed rectifier K^+ current in rabbit sinoatrial and atrioventricular node cells. *Eur. J. Pharmacol.* 404:281-288.
14. Mitcheson, J. S. and J. C. Hancox. 1999. Characteristics of a transient outward current (sensitive to 4-aminopyridine) in Ca^{2+}-tolerant myocytes isolated from the rabbit atrioventricular node. *Pflügers Arch*. 438:68-78.
15. Howarth, F. C., A. J. Levi, and J. C. Hancox. 1996. Characteristics of the delayed rectifier K current compared in myocytes isolated from the atrioventricular node and ventricle of the rabbit heart. *Pflügers Arch.* 431:713-722.
16. Mitcheson, J. S. and J. C. Hancox. 1999. An investigation of the role played by the E-4031-sensitive (rapid delayed rectifier) potassium current in isolated rabbit atrioventricular nodal and ventricular myocytes. *Pflügers Arch.* 438:843-850.
17. Lei, M., H. Honjo, I. Kodama, and M. R. Boyett. 2001. Heterogeneous expression of the delayed-rectifier K^+ currents $i_{K,r}$ and $i_{K,s}$ in rabbit sinoatrial node cells. *J. Physiol*. 535:703-714.
18. Habuchi, Y., X. Han, and W. R. Giles. 1995. Comparison of the hyperpolarisation-activated and delayed rectifier current in rabbit atrioventricular node and sinoatrial node. *Heart and Vessels*. S9:203-206.
19. Dobrzynski, H., V. P. Nikolski, A. T. Sambelashvili, I. D. Greener, M. Yamamoto, M. R. Boyett, and I. R. Efimov. 2003. Site of origin and molecular substrate of atrioventricular junctional rhythm in the rabbit heart. *Circ. Res.* 93:1102-1110.
20. Nakayama, T., Y. Kurachi, A. Noma, and H. Irisawa. 1984. Action potential and membrane currents of single pacemaker cells of the rabbit heart. *Pflügers Arch.* 402:248-257.
21. Hancox, J. and A. Levi. 1994. The hyperpolarisation-activated current, I_f, is not required for pacemaking in single cells from the rabbit atrioventricular node. *Pflügers Arch.* 427:121-128.
22. Kurata, Y., I. Hisatome, S. Imanishi, and T. Shibamoto. 2002. Dynamical description of sinoatrial node pacemaking: improved mathematical model for primary pacemaker cell. *Am. J. Physiol*. 283:H2074-H2101.
23. Hancox, J. C., A. J. Levi, C. O. Lee, and P. Heap. 1993. A method for isolating rabbit

atrioventricular node myocytes which retain normal morphology and function. *Am. J. Physiol*. 265:H755-H766.

24. Noma, A., T. Nakayama, Y. Kurachi, and H. Irisawa. 1984. Resting K conductances in pacemaker and non-pacemaker heart cells of the rabbit. *Jpn. J. Physiol*. 34:245-254.
25. Dobrzynski, H., R. Billeter, I. D. Greener, J. O. Tellez, N. J. Chandler, T. P. Flagg, C. G. Nichols, A. N. Lopatin, and M. R. Boyett. 2006. Expression of Kir2.1 and Kir6.2 transgenes under the control of the α-MHC promoter in the sinoatrial and atrioventricular nodes in transgenic mice. *J. Mol. Cell. Cardiol*. 41:855-867.
26. Convery, M. K. and J. C. Hancox. 2000. Na^{+}-Ca^{2+} exchange current from rabbit isolated atrioventricular nodal and ventricular myocytes compared using action potential and ramp waveforms. *Acta Phsiologica Scandinavica.* 168:393-401.
27. Ho, W. K., W. G. Kim, and Y. E. Earm. 1986. Membrane currents in the atrioventricular node of the rabbit. *Seoul J. Med.* 27:211-231.
28. Zhang, H., A. V. Holden, I. Kodama, H. Honjo, M. Lei, T. Varghese, and M. R. Boyett. 2000. Mathematical models of action potentials in the periphery and center of the rabbit sinoatrial node. *Am. J. Physiol*. 279:H397-H421.
29. Bogdanov, K. Y., T. M. Vinogradova, and E. G. Lakatta. 2001. Sinoatrial nodal cell ryanodine receptor and Na^{+}-Ca^{2+} exchanger: molecular partners in pacemaker regulation. *Circ. Res.* 88:1254-1258.
30. Janvier, N. C., S. M. Harrison, and M. R. Boyett. 1997. The role of inward Na^{+}-Ca^{2+} exchange current in the ferret ventricular action potential. *J. Physiol*. 498:611-625.
31. Nikmaram, M. R., J. Liu, M. Abdelrahman, H. Dobrzynski, M. R. Boyett, and M. Lei. 2008. Characterization of the effects of ryanodine, TTX, E-4031 and 4-AP on the sinoatrial and atrioventricular nodes. *Prog. Biophys. Mol. Biol.* 96:452-464.
32. Zhang, H., A. V. Holden, and M. R. Boyett. 2001. Gradient model versus mosaic model of the sinoatrial node. *Circulation*. 103:584-588.
33. Hancox, J. C. 1997. Amiodarone blocks L-type calcium current in single myocytes isolated from the rabbit atrioventricular node. *Gen. Pharmacol.* 29:429-435.
34. Liu, Y., W. Zeng, M. Delmar, and J. Jalife. 1993. Ionic mechanisms of electronic inhibition and concealed conduction in rabbit atrioventricular nodal myocytes. *Circulation*. 88:1634-1646.
35. Workman, A. J., K. A. Kane, and A. C. Rankin. 1999. Ionic basis of a differential effect of adenosine on refractoriness in rabbit AV nodal and atrial isolated myocytes. *Cardiovasc. Res.* 43:974-984.
36. Shibasaki, T. 1987. Conductance and kinetics of delayed rectifier potassium channels in nodal cells of the rabbit heart. *J. Physiol*. 387:227-250.
37. Kokubun, S., M. Nishimura, A. Noma, and H. Irisawa. 1982. Membrane currents in the rabbit atrioventricular node cell. *Pflügers Arch.* 393:15-22.
38. Hancox, J. C., A. J. Levi, and P. Brooksby. 1994. Intracellular calcium transients recorded with Fura-2 in spontaneously active myocytes isolated from the atrioventricular node of the

rabbit heart. *Proc. Biol. Sci.* 255:99-105.

Figure legends

Figure S1. Comparison of the model of the L-type Ca^{2+} current ($I_{Ca,L}$) with experimental data. In A-E and G, symbols show experimental data and lines were generated by the model. A, activation curves for $I_{Ca,L}$. The activation curve was assumed to be shifted in N cells to more negative potentials – see text. B, inactivation curve for $I_{Ca,L}$. C and D, time constants of fast and slow inactivation of $I_{Ca,L}$. E, normalised current-voltage relationships for $I_{Ca,L}$. The current-voltage relationship for N cells is shifted as a result of the shift of the activation curve. F, recovery of $I_{Ca,L}$ from inactivation. Superimposed records of $I_{Ca,L}$ from the N cell model are shown. $I_{Ca,L}$ was activated during 1 s control and 300 ms test pulses to +20 mV from a holding potential of -40 mV. The interval between the control and test pulses was varied in different runs. G, time course of recovery of $I_{Ca,L}$ from inactivation. Data from experiments like that in F; the amplitude of $I_{Ca,L}$ during the test pulse (as a percentage of that in the control pulse) is plotted against the interval between the control and test pulses. Recovery from inactivation at holding potentials of -40 mV (solid line and all experimental data) and -60 mV (dashed line) is shown. H, $I_{Ca,L}$ at +10 mV from a holding potential of -40 mV from simulation (AN cell model used; top) and experiment (33) (bottom). Filled circle (34); filled square (8); filled triangle (9); inverted filled triangle (33); filled diamond (11); pentagon (12); + (13); × (20); asterisk (35).

Figure S2. Comparison of the model of the transient outward current (I_{to}) with experimental data. In A-D, F and H, symbols show experimental data and lines were generated by model. A and B, activation and inactivation curves for $I_{to,fast}/I_{to,slow}$. C and D, time constants of inactivation of $I_{to,fast}$ (C) and $I_{to,slow}$ (D). E, superimposed records of I_{to} ($I_{to,fast} + I_{to,slow}$) during 500 ms pulses to -10 to +40 mV from a holding potential of −80 mV from simulation (AN cell model used; left) and experiment (14) (right). F, normalised current-voltage relationships for I_{to} ($I_{to,fast}$ + $I_{to,slow}$). Data from experiments like that in E. G, recovery of I_{to} ($I_{to,fast}$ + $I_{to,slow}$) from inactivation. Superimposed records of computed I_{to} ($I_{to,fast}$ + $I_{to,slow}$) from the AN cell model are shown. I_{to} ($I_{to,fast}$ + $I_{to,slow}$) was activated during 500 ms control and test pulses to +40 mV from a holding potential of −80 mV. The interval between the control and test pulses was varied in different runs. H, time course of recovery of I_{to} ($I_{to,fast}$ + $I_{to,slow}$) from inactivation. Data from experiments like that in G; the amplitude of I_{to} ($I_{to,fast}$ + $I_{to,slow}$) during the test pulse (as a percentage of that in the control pulse) is plotted against the interval between the control and test pulses. Filled circle (7); filled square (14).

Figure S3. Comparison of the model of the rapid delayed rectifier K^+ current ($I_{K,r}$) with experimental data. In A-D, symbols show experimental data and lines were generated by model. A, activation curve for $I_{K,r}$. B, time constants of activation of $I_{K,r}$. C and D, normalised current-voltage relationships for $I_{K,r}$ at the end of the pulse (C) and tail current (D). For C, computed $I_{K,r}$ was measured at the end of 500 ms pulses to -10 to +30 mV from a holding potential of −40 mV and, for D, the peak amplitude of $I_{K,r}$ tail current was measured after the pulse. Experimentally, $I_{K,r}$ was measured using the same protocols. E, $I_{K,r}$ during 500 ms pulses to -10 to +30 mV from a holding potential of −40 mV from simulation (N cell model used; left) and experiment (16) (right). Open circle (15); open square (36); open triangle (16); inverted open triangle (13).

Figure S4. Comparison of the model of the hyperpolarization-activated current (I_f) with experimental data. In A-C, symbols show experimental data and lines were generated by the model. A, activation curve of I_f. B, time constants of activation of I_f. C, current-voltage relationship for I_f. Data from experiments like that in D. D, superimposed records of I_f during 4 s pulses to -60 to -120 mV from a holding potential of -50 mV from simulation (N cell model used; left) and experiment (rabbit ovoid cell (1); right). Open circle (21); open square (1); open triangle (37).

Figure S5. Sustained inward current. A, activation curve for I_{st}. B, I_{st} in the N cell model. I_{st} was recorded during 500 ms pulses to potentials between -80 and +60 mV (in 10 mV increments) from a holding potential of -80 mV. C, current-voltage relationship for I_{st} (from experiments like that in B).

Figure S6. Na^{+}-Ca^{2+} exchanger current (I_{NaCa}). A, I_{NaCa} (top) recorded during voltage clamp ramp (bottom). I_{NaCa} from simulations (solid lines) and experiment (dashed line) shown. B, current-voltage relationships for I_{NaCa} from simulations (solid lines) and experiment (squares). Experimental data from Convery and Hancox. (26).

Figure S7. Action potentials (top) and intracellular Ca^{2+} transients (bottom) predicted by the atrial and AVN models. The Ca^{2+} transient shown by the dashed line was recorded from a spontaneous AVN cell isolated from the rabbit (38). The experimental recording was in arbitrary units and has been superimposed on the simulated Ca^{2+} transient.

Data file legends

Data file 1. const.h. Values of constants.

Data file 2. cell_base.h. Common file for models.

Data file 3. atrium.h. Header file for atrial cell model.

Data file 4. atrium.cpp. Atrial cell model.

Data file 5. av_node_2.h. Header file for AVN cell model.

Data file 6. av_node_2.cpp. AVN model.

Data file 7. solution.cpp. Function for solving differential equations.

Table S1. Glossary.

General	V	Transmembrane potential
	C_m	Membrane capacitance
	t	Time
	$g(i, j)$	Coupling conductance between i^{th} and j^{th} cell
	I_{total}	Total ionic current
	I_{Na}	Na^+ current
	$I_{Ca,L}$	L-type Ca^{2+} current
	I_{to}	Transient outward K^+ current
	$I_{K,r}$	Rapid delayed rectifier K^+ current
	I_f	Hyperpolarization-activated current
	I_{st}	Sustained inward current
	I_p	Na^+-K^+ pump current
	$I_{Na,Ca}$	Na^+-Ca^{2+} exchanger current
	I_b	Background current
	$I_{K,1}$	Inward rectifier K^+ current
	$[Na^+]_i$, $[Ca^{2+}]_i$, $[K^+]_i$	Intracellular Na^+, Ca^{2+} and K^+ concentrations
	$[Na^+]_o$, $[Ca^{2+}]_o$, $[K^+]_o$	Extracellular Na^+, Ca^{2+} and K^+ concentrations
	$[Ca^{2+}]_{rel}$	Ca^{2+} concentration in junctional sarcoplasmic reticulum
	$[Ca^{2+}]_{sub}$	Subspace Ca^{2+} concentration
	$[Ca^{2+}]_{up}$	Ca^{2+} concentration in network sarcoplasmic reticulum
	$[Mg^{2+}]_i$	Intracellular Mg^{2+} concentration
	F	Faraday's constant (96500 C/mol)
	R	Universal gas constant (8.31 J/(mol·K))
	T	Absolute temperature (310 K)
	V_i	Myoplasmic volume
	V_{rel}	Volume of junctional sarcoplasmic reticulum
	V_{sub}	Subspace volume
	V_{up}	Volume of network sarcoplasmic reticulum

Table S1. Glossary (continued).

$\boldsymbol{I_{\mathrm{Na}}}$	m	Activation variable for I_{Na}
	α_m	Voltage-dependent opening rate constant of m
	β_m	Voltage-dependent closing rate constant of m
	h_{total}, h_1, h_2	Inactivation variables for I_{Na}
	α_h	Voltage-dependent opening rate constant of h_1 and h_2
	β_h	Voltage-dependent closing rate constant of h_1 and h_2
	τ_{h1}, τ_{h2}	Voltage-dependent time constants of h_1 and h_2
	$h_{1\infty}$, $h_{2\infty}$	Voltage-dependent steady-state values of h_1 and h_2
	P_{Na}	Na^+ permeability for I_{Na}
	g_{Na}	Na^+ conductance for I_{Na}
$\boldsymbol{I_{\mathrm{Ca,L}}}$	d_{L}	Activation variable for $I_{\mathrm{Ca,L}}$
	$\alpha_{d\mathrm{L}}$	Voltage-dependent opening rate constant of d_{L}
	$\beta_{d\mathrm{L}}$	Voltage-dependent closing rate constant of d_{L}
	$\tau_{d\mathrm{L}}$	Voltage-dependent time constant of d_{L}
	$d_{\mathrm{L}\infty}$	Voltage-dependent steady-state value of d_{L}
	$f_{\mathrm{L,fast}}$, $f_{\mathrm{L,slow}}$	Inactivation variables for $I_{\mathrm{Ca,L}}$
	$\tau_{f\mathrm{L,fast}}$, $\tau_{f\mathrm{L,slow}}$	Voltage-dependent time constants of $f_{\mathrm{L,fast}}$ and $f_{\mathrm{L,slow}}$
	$f_{\mathrm{L,\ fast}\infty}$, $f_{\mathrm{L,slow}\infty}$	Voltage-dependent steady-state values of $f_{\mathrm{L,fast}}$ and $f_{\mathrm{L,slow}}$
	$g_{\mathrm{Ca,L}}$	Conductance for $I_{\mathrm{Ca,L}}$
	$E_{\mathrm{Ca,L}}$	Reversal potential for $I_{\mathrm{Ca,L}}$
$\boldsymbol{I_{\mathrm{to}}}$	r	Activation variable for I_{to}
	r_∞	Voltage-dependent steady-state value of r
	τ_r	Voltage-dependent time constant of r
	q	Inactivation variable for I_{to}
	q_∞	Voltage-dependent steady-state value of q
	$\tau_{q\mathrm{fast}}$, $\tau_{q\mathrm{slow}}$	Voltage-dependent time constants of q
	g_{to}	Conductance for I_{to}

Table S1. Glossary (continued).

$\boldsymbol{I_{K,r}}$	$p_{a,fast}$, $p_{a,slow}$	Activation variables for $I_{K,r}$
	$p_{a,fast\infty}$	Voltage-dependent steady-state value of $p_{a,fast}$
	$\tau_{pa,fast}$	Voltage-dependent time constant of $p_{a,fast}$
	$p_{a,slow\infty}$	Voltage-dependent steady-state value of $p_{a,slow}$
	$\tau_{pa,slow}$	Voltage-dependent time constant of $p_{a,fast}$
	p_i	Inactivation variable for $I_{K,r}$
	α_{pi}	Voltage-dependent opening rate constant of p_i
	β_{pi}	Voltage-dependent closing rate constant of p_i
	τ_{pi}	Voltage-dependent time constant of p_i
	$p_{i\infty}$	Voltage-dependent steady-state value of p_i
	$g_{K,r}$	Conductance for $I_{K,r}$
$\boldsymbol{I_f}$	y	Activation variable for I_f
	y_∞	Voltage-dependent steady-state value of y
	τ_y	Voltage-dependent time constant of y
	g_f	Conductance for I_f
$\boldsymbol{I_{st}}$	q_a	Activation variable for I_{st}
	$q_{a\infty}$	Voltage-dependent steady-state value of q_a
	τ_{qa}	Voltage-dependent time constant of q_a
	q_i	Inactivation variable for I_{st}
	$q_{i\infty}$	Voltage-dependent steady-state value of q_i
	τ_{qi}	Voltage-dependent time constant of q_i
	g_{st}	Conductance for I_{st}

Table S1. Glossary (continued).

$\boldsymbol{I_{Na,Ca}}$	d_i	Common denominator for the E1 state
	d_o	Common denominator for the E2 state
	K_{1ni}	Dissociation constant for intracellular Na^+ binding to first site on I_{NaCa} transporter
	K_{2ni}	Dissociation constant for intracellular Na^+ binding to second site on I_{NaCa} transporter
	K_{3ni}	Dissociation constant for intracellular Na^+ binding to third site on I_{NaCa} transporter
	K_{1no}	Dissociation constant for extracellular Na^+ binding to first site on I_{NaCa} transporter
	K_{2no}	Dissociation constant for extracellular Na^+ binding to second site on I_{NaCa} transporter
	K_{3no}	Dissociation constant for extracellular Na^+ binding to third site on I_{NaCa} transporter
	Q_{ci}	Fractional charge movement during intracellular Ca^{2+} occlusion reaction of I_{NaCa} transporter
	Q_{co}	Fractional charge movement during extracellular Ca^{2+} occlusion reaction of I_{NaCa} transporter
	Q_n	Fractional charge movement during Na^+ occlusion reactions of I_{NaCa} transporter
	k_{12}	Rate constant for the E1 to E2 transition
	k_{14}	Rate constant for the E1 to E4 transition
	k_{21}	Rate constant for the E2 to E1 transition
	k_{23}	Rate constant for the E2 to E3 transition
	k_{32}	Rate constant for the E3 to E2 transition
	k_{34}	Rate constant for the E3 to E4 transition
	k_{41}	Rate constant for the E4 to E1 transition
	k_{43}	Rate constant for the E4 to E3 transition
	x_1	Temporary variable for the E1 state
	x_2	Temporary variable for the E2 state
	x_3	Temporary variable for the E3 state
	x_4	Temporary variable for the E4 state
	k_{NaCa}	Scaling factor for I_{NaCa}

Table S1. Glossary (continued).

$\boldsymbol{I_p}$	$\overline{I}_p$	Maximum I_p
	$K_{m,\,Na}$, $K_{m,K}$	Dissociation constants for Na^+ and K^+ activation of I_p
$\boldsymbol{I_b}$	g_b	Conductance for I_b
	E_b	Reversal potential for I_b
Ca^{2+}-handling	$j_{Ca,dif}$	Ca^{2+} diffusion flux from subspace to myoplasm
	j_{rel}	Ca^{2+} release flux from the junctional SR to subspace
	j_{up}	Ca^{2+} uptake flux from the myoplasm to network SR
	j_{tr}	Ca^{2+} transfer flux from the network to junctional SR
	f_{TC}	Fractional occupancy of the troponin-Ca^{2+} site by Ca^{2+}
	f_{TMC}	Fractional occupancy of the troponin-Mg^{2+} site by Ca^{2+}
	f_{TMM}	Fractional occupancy of the troponin-Mg^{2+} site by Mg^{2+}
	f_{CMi}	Fractional occupancy of calmodulin by Ca^{2+} in myoplasm
	f_{CMs}	Fractional occupancy of calmodulin by Ca^{2+} in subspace
	f_{CQ}	Fractional occupancy of calsequestrin by Ca^{2+}
	f_{CSL}	Fractional occupancy of calmodulin by Ca^{2+} in the sarcolemma
	$\tau_{diff,Ca}$	Time constant of Ca^{2+} diffusion from the subspace to myoplasm
	τ_{tr}	Time constant for Ca^{2+} transfer from the network to junctional SR
	P_{rel}	Rate constant for Ca^{2+} release from the junctional SR
	P_{up}	Rate constant for Ca^{2+} uptake by the Ca^{2+} pump in the network SR
	K_{rel}	Half-maximal $[Ca^{2+}]_{sub}$ for Ca^{2+} release from the junctional SR
	K_{up}	Half-maximal $[Ca^{2+}]_i$ for Ca^{2+} uptake by the Ca^{2+} pump in the network SR
	$[CM]_{tot}$	Total calmodulin concentration
	$[TC]_{tot}$	Total concentration of the troponin-Ca^{2+} site
	$[TMC]_{tot}$	Total concentration of the troponin-Mg^{2+} site
	$[CQ]_{tot}$	Total calsequestrin concentration
	k_{fTC}	Ca^{2+} association constant for troponin

Table S1. Glossary (continued).

	$k_{b\mathrm{TC}}$	Ca^{2+} dissociation constant for the troponin-Ca^{2+} site
	$k_{f\mathrm{TMC}}$	Ca^{2+} association constant for the troponin-Mg^{2+} site
	$k_{b\mathrm{TMC}}$	Ca^{2+} dissociation constant for the troponin-Mg^{2+} site
	$k_{f\mathrm{TMM}}$	Mg^{2+} association constant for the troponin-Mg^{2+} site
	$k_{b\mathrm{TMM}}$	Mg^{2+} dissociation constant for the troponin-Mg^{2+} site
	$k_{f\mathrm{CM}}$	Ca^{2+} association constant for calmodulin
	$k_{b\mathrm{CM}}$	Ca^{2+} dissociation constant for calmodulin
	$k_{f\mathrm{CQ}}$	Ca^{2+} association constant for calsequestrin
	$k_{b\mathrm{CQ}}$	Ca^{2+} dissociation constant for calsequestrin
1D model	n	Cell number
	$C_{\mathrm{m,SAN}}(n)$	Cell capacitance of n^{th} SAN cell
	$C_{\mathrm{m,AM}}(n)$	Cell capacitance of n^{th} AM cell
	$C_{\mathrm{m,FP}}(n)$	Cell capacitance of n^{th} cell in fast pathway
	$C_{\mathrm{m,SP}}(n)$	Cell capacitance of n^{th} cell in slow pathway
	$C_{\mathrm{m,NH}}(n)$	Cell capacitance of n^{th} cell nodal His region
	$g_{\mathrm{SAN}}(n, n+1)$	Coupling conductance of n^{th} SAN cell
	$g_{\mathrm{AM}}(n, n+1)$	Coupling conductance of n^{th} AM cell
	$g_{\mathrm{FP}}(n, n+1)$	Coupling conductance of n^{th} cell in fast pathway
	$g_{\mathrm{SP}}(n, n+1)$	Coupling conductance of n^{th} cell in slow pathway
	$g_{\mathrm{NH}}(n, n+1)$	Coupling conductance of n^{th} cell in nodal His region
	$P_{\mathrm{Na,AM}}(n)$	Na^{+} permeability of n^{th} AM cell
	$P_{\mathrm{Na,FP}}(n)$	Na^{+} permeability of n^{th} cell in fast pathway
	$P_{\mathrm{Na,SP}}(n)$	Na^{+} permeability of n^{th} cell in slow pathway
	$P_{\mathrm{Na,NH}}(n)$	Na^{+} permeability of n^{th} cell in nodal His region

Table S2. General equations.

$$I_{\text{total}} = \begin{cases} I_{\text{Na}} + I_{\text{Ca,L}} + I_{\text{to}} + I_{\text{K,r}} + I_{\text{f}} + I_{\text{st}} + I_{\text{K,1}} + I_{\text{NaCa}} + I_{\text{p}} + I_{\text{b}} & (\text{AN, N, NH}) \\ I_{\text{Na}} + I_{\text{Ca,L}} + I_{\text{Ca,T}} + I_{\text{to}} + I_{\text{K,r}} + I_{\text{K,s}} + I_{\text{K,1}} + I_{\text{b}} + I_{\text{NaK}} + I_{\text{NaCa}} + I_{\text{CaP}} & (\text{AM}) \end{cases} \tag{1}$$

$$\frac{\mathrm{d}V(i)}{\mathrm{d}t} = -\frac{1}{C_{\text{m}}(i)}\left(I_{\text{total}} + \sum_j g(i, j)\{V(i) - V(j)\} \right) \tag{2}$$

Table S3. I_{Na}.

$$\alpha_m(V) = \frac{-460.0(V+44.4)}{\exp((V+44.4)/-12.673)-1.0} \tag{1}$$

$$\beta_m(V) = 18400.0\exp((V+44.4)/-12.673) \tag{2}$$

$$\frac{\mathrm{d}m}{\mathrm{d}t} = \alpha_m(1-m) - \beta_m m \tag{3}$$

$$\alpha_h(V) = 44.9\exp((V+66.9)/-5.57) \tag{4}$$

$$\beta_h(V) = \frac{1491.0}{1.0+323.3\exp((V+94.6)/-12.9)} \tag{5}$$

$$\tau_{h_1}(V) = \frac{0.03}{1.0+\exp((V+40.0)/6.0)} + 0.00035 \tag{6}$$

$$h_{1\infty} = \alpha_h/(\alpha_h+\beta_h) \tag{7}$$

$$\frac{\mathrm{d}h_1}{\mathrm{d}t} = \frac{h_{1\infty}-h_1}{\tau_{h_1}} \tag{8}$$

$$h_{2\infty} = h_{1\infty} \tag{9}$$

$$\tau_{h_2}(V) = \frac{0.12}{1.0+\exp((V+60.0)/2.0)} + 0.00295 \tag{10}$$

$$\frac{\mathrm{d}h_2}{\mathrm{d}t} = \frac{h_{2\infty}-h_2}{\tau_{h_2}} \tag{11}$$

$$h_{\text{total}} = 0.635h_1 + 0.365h_2 \tag{12}$$

$$g_{\text{Na}} = P_{\text{Na}}[\text{Na}^+]_{\text{o}}F^2/(RT) \tag{13}$$

$$I_{\text{Na}} = g_{\text{Na}}m^3h_{\text{total}}V\frac{\exp[(V-E_{\text{Na}})F/(RT)]-1.0}{\exp[VF/(RT)]-1.0} \tag{14}$$

Table S4. $I_{\mathrm{Ca,L}}$.

$$d_{\mathrm{L}\infty}(V)=\begin{cases}\dfrac{1.0}{1.0+\exp((V+3.2)/-6.61)} & (\mathrm{AN,NH})\\[2ex] \dfrac{1.0}{1.0+\exp((V+18.2)/-5.0)} & (\mathrm{N})\end{cases} \tag{1}$$

$$\alpha_{d_\mathrm{L}}(V)=\frac{-26.12(V+35.0)}{\exp((V+35.0)/-2.5)-1.0}+\frac{-78.11V}{\exp(-0.208V)-1.0} \tag{2}$$

$$\beta_{d_\mathrm{L}}(V)=\frac{10.52(V-5.0)}{\exp(0.4(V-5.0))-1.0} \tag{3}$$

$$\tau_{d_\mathrm{L}}=1.0/(\alpha_{d_\mathrm{L}}+\beta_{d_\mathrm{L}}) \tag{4}$$

$$\frac{\mathrm{d}d_\mathrm{L}}{\mathrm{d}t}=\frac{d_{\mathrm{L}\infty}-d_\mathrm{L}}{\tau_{d_\mathrm{L}}} \tag{5}$$

$$f_{\mathrm{L,fast}\infty}(V)=f_{\mathrm{L,slow}\infty}(V)=\frac{1.0}{1.0+\exp((V+29.0)/6.31)} \tag{6}$$

$$\tau_{f_\mathrm{L,fast}}(V)=0.010+0.1539\exp\left(-(V+40.0)^2/185.67\right) \tag{7}$$

$$\tau_{f_\mathrm{L,slow}}(V)=0.060+1.08171\exp\left(-(V+40.0)^2/138.04\right) \tag{8}$$

$$\frac{\mathrm{d}f_\mathrm{L,fast}}{\mathrm{d}t}=\frac{f_{\mathrm{L,fast}\infty}-f_\mathrm{L,fast}}{\tau_{f_\mathrm{L,fast}}} \tag{9}$$

$$\frac{\mathrm{d}f_\mathrm{L,slow}}{\mathrm{d}t}=\frac{f_{\mathrm{L,slow}\infty}-f_\mathrm{L,slow}}{\tau_{f_\mathrm{L,slow}}} \tag{10}$$

$$I_\mathrm{Ca,L}=g_\mathrm{Ca,L}d_\mathrm{L}(0.675f_\mathrm{L,fast}+0.325f_\mathrm{L,slow})(V-E_\mathrm{Ca,L}) \tag{11}$$

Table S5. I_{to}.

$$r_\infty(V) = \frac{1.0}{1.0 + \exp((V - 7.44)/-16.4)} \tag{1}$$

$$\tau_r(V) = \left(0.596 \times 10^{-3}\right) + \frac{3.188 \times 10^{-3}}{1.037\exp(0.09(V + 30.61)) + 0.396\exp(-0.12(V + 23.84))} \tag{2}$$

$$\frac{\mathrm{d}r}{\mathrm{d}t} = \frac{r_\infty - r}{\tau_r} \tag{3}$$

$$q_\infty(V) = \frac{1.0}{1.0 + \exp((V + 33.8)/6.12)} \tag{4}$$

$$\tau_{q_{\text{fast}}}(V) = 0.1266 + \frac{4.72716}{1.0 + \exp((V + 154.5)/23.96)} \tag{5}$$

$$\tau_{q_{\text{slow}}}(V) = 0.100 + 4.000\exp\left(-(V + 65.0)^2/500.0\right) \tag{6}$$

$$\frac{\mathrm{d}q_{\text{fast}}}{\mathrm{d}t} = \frac{q_\infty - q_{\text{fast}}}{\tau_{q_{\text{fast}}}} \tag{7}$$

$$\frac{\mathrm{d}q_{\text{slow}}}{\mathrm{d}t} = \frac{q_\infty - q_{\text{slow}}}{\tau_{q_{\text{slow}}}} \tag{8}$$

$$I_{\text{to}} = g_{\text{to}} r(0.45q_{\text{fast}} + 0.55q_{\text{slow}})(V - E_{\text{K}}) \tag{9}$$

Table S6. $I_{\mathrm{K,r}}$.

$$p_{\mathrm{a,fast}\infty}(V)=\frac{1.0}{1.0+\exp((V+10.22)/-8.50)} \tag{1}$$

$$\tau_{p_{\mathrm{a,fast}}}(V)=\frac{1.0}{17.0\exp(0.0398V)+0.211\exp(-0.0510V)} \tag{2}$$

$$\frac{\mathrm{d}p_{\mathrm{a,fast}}}{\mathrm{d}t}=\frac{p_{\mathrm{a,fast}\infty}-p_{\mathrm{a,fast}}}{\tau_{p_{\mathrm{a,fast}}}} \tag{3}$$

$$p_{\mathrm{a,slow}\infty}=p_{\mathrm{a,fast}\infty} \tag{4}$$

$$\tau_{p_{\mathrm{a,slow}}}(V)=0.33581+0.90673\exp\left(-(V+10.00)^2/988.05\right) \tag{5}$$

$$\frac{\mathrm{d}p_{\mathrm{a,slow}}}{\mathrm{d}t}=\frac{p_{\mathrm{a,slow}\infty}-p_{\mathrm{a,slow}}}{\tau_{p_{\mathrm{a,slow}}}} \tag{6}$$

$$p_{\mathrm{i}\infty}(V)=\frac{1.0}{1.0+\exp((V+4.90)/15.14)}\left(1.0-0.3\exp\left(-V^2/500.0\right)\right) \tag{7}$$

$$\alpha_{p_{\mathrm{i}}}(V)=92.01\exp(-0.0183V) \tag{8}$$

$$\beta_{p_{\mathrm{i}}}(V)=603.6\exp(0.00942V) \tag{9}$$

$$\tau_{p_{\mathrm{i}}}=1.0/\left(\alpha_{p_{\mathrm{i}}}+\beta_{p_{\mathrm{i}}}\right) \tag{10}$$

$$\frac{\mathrm{d}p_{\mathrm{i}}}{\mathrm{d}t}=\frac{p_{\mathrm{i}\infty}-p_{\mathrm{i}}}{\tau_{p_{\mathrm{i}}}} \tag{11}$$

$$I_{\mathrm{K,r}}=g_{\mathrm{K,r}}\left(0.90\,p_{\mathrm{a,fast}}+0.10\,p_{\mathrm{a,slow}}\right)p_{\mathrm{i}}(V-E_{\mathrm{K}}) \tag{12}$$

Table S7. $\boldsymbol{I_\mathrm{f}}$**.**

$$y_\infty(V) = \frac{1.0}{1.0 + \exp((V - (-83.19))/13.56)} \tag{1}$$

$$\tau_y(V) = 0.250 + 2.000\exp\left(-(V - (-70.00))^2/500.0\right) \tag{2}$$

$$\frac{\mathrm{d}y}{\mathrm{d}t} = \frac{y_\infty - y}{\tau_y} \tag{3}$$

$$I_\mathrm{f} = g_\mathrm{f}\, y(V - (-30.00)) \tag{4}$$

Table S8. $\boldsymbol{I_\mathrm{st}}$**.**

$$q_{\mathrm{a}\infty}(V) = \frac{1.0}{1.0 + \exp((V - (-49.10))/-8.98)} \tag{1}$$

$$\alpha_{q\mathrm{a}}(V) = \frac{1.0}{0.15\exp(-V/11.0) + 0.2\exp(V/700.0)} \tag{2}$$

$$\beta_{q\mathrm{a}}(V) = \frac{1.0}{16.0\exp(V/8.0) + 15.0\exp(V/50.0)} \tag{3}$$

$$\tau_{q\mathrm{a}} = 1.0/(\alpha_{q\mathrm{a}} + \beta_{q\mathrm{a}}) \tag{4}$$

$$\frac{\mathrm{d}q_\mathrm{a}}{\mathrm{d}t} = \frac{q_{\mathrm{a}\infty} - q_\mathrm{a}}{\tau_{q\mathrm{a}}} \tag{5}$$

$$\alpha_{q\mathrm{i}}(V) = \frac{0.1504}{3100.0\exp(V/13.0) + 700.0\exp(V/70.0)} \tag{6}$$

$$\beta_{q\mathrm{i}}(V) = \frac{0.1504}{95.0\exp(-V/10.0) + 50.0\exp(-V/700.0)} + \frac{0.000229}{1.0 + \exp(-V/5.0)} \tag{7}$$

$$q_{\mathrm{i}\infty} = \alpha_{q\mathrm{i}}/(\alpha_{q\mathrm{i}} + \beta_{q\mathrm{i}}) \tag{8}$$

$$\tau_{q\mathrm{i}} = 1.0/(\alpha_{q\mathrm{i}} + \beta_{q\mathrm{i}}) \tag{9}$$

$$\frac{\mathrm{d}q_\mathrm{i}}{\mathrm{d}t} = \frac{q_{\mathrm{i}\infty} - q_\mathrm{i}}{\tau_{q\mathrm{i}}} \tag{10}$$

$$I_\mathrm{st} = g_\mathrm{st} q_\mathrm{a} q_\mathrm{i}(V - E_\mathrm{st}) \tag{11}$$

Table S9. $\boldsymbol{I_\mathrm{K,1}}$**.**

$$g'_\mathrm{K,1} = g_\mathrm{K,1}\left(0.5 + \frac{0.5}{1.0 + \exp((V - (-30.0))/-5.0)}\right) \tag{1}$$

$$I_\mathrm{K,1} = g'_\mathrm{K,1}\left(\frac{[\mathrm{K}^+]_\mathrm{o}}{[\mathrm{K}^+]_\mathrm{o} + 0.590}\right)^3 \frac{V - (-81.9)}{1.0 + \exp\{1.393(V - (-81.9) + 3.6)F/(RT)\}} \tag{2}$$

Table S10. $\boldsymbol{I_{\mathrm{NaCa}}}$.

$$d_{\mathrm{i}} = 1 + \frac{[\mathrm{Ca}^{2+}]_{\mathrm{sub}}}{K_{\mathrm{ci}}}\left\{1 + \exp\left(-\frac{Q_{\mathrm{ci}}VF}{RT}\right) + \frac{[\mathrm{Na}^+]_{\mathrm{i}}}{K_{\mathrm{cni}}}\right\} + \frac{[\mathrm{Na}^+]_{\mathrm{i}}}{K_{1\mathrm{ni}}}\left\{1 + \frac{[\mathrm{Na}^+]_{\mathrm{i}}}{K_{2\mathrm{ni}}}\left(1 + \frac{[\mathrm{Na}^+]_{\mathrm{i}}}{K_{3\mathrm{ni}}}\right)\right\} \tag{1}$$

$$d_{\mathrm{o}} = 1 + \frac{[\mathrm{Ca}^{2+}]_{\mathrm{o}}}{K_{\mathrm{co}}}\left\{1 + \exp\left(\frac{Q_{\mathrm{co}}VF}{RT}\right)\right\} + \frac{[\mathrm{Na}^+]_{\mathrm{o}}}{K_{1\mathrm{no}}}\left\{1 + \frac{[\mathrm{Na}^+]_{\mathrm{o}}}{K_{2\mathrm{no}}}\left(1 + \frac{[\mathrm{Na}^+]_{\mathrm{o}}}{K_{3\mathrm{no}}}\right)\right\} \tag{2}$$

$$k_{43} = [\mathrm{Na}^+]_{\mathrm{i}} / \left(K_{3\mathrm{ni}} + [\mathrm{Na}^+]_{\mathrm{i}}\right) \tag{3}$$

$$k_{12} = \left([\mathrm{Ca}^{2+}]_{\mathrm{sub}} / K_{\mathrm{ci}}\right)\exp\left(-Q_{\mathrm{ci}}VF / (RT)\right) / d_{\mathrm{i}} \tag{4}$$

$$k_{14} = \frac{1}{d_{\mathrm{i}}}\frac{[\mathrm{Na}^+]_{\mathrm{i}}}{K_{1\mathrm{ni}}}\frac{[\mathrm{Na}^+]_{\mathrm{i}}}{K_{2\mathrm{ni}}}\left(1 + \frac{[\mathrm{Na}^+]_{\mathrm{i}}}{K_{3\mathrm{ni}}}\right)\exp\left(-\frac{Q_{\mathrm{n}}VF}{2RT}\right) \tag{5}$$

$$k_{41} = \exp\left(-Q_{\mathrm{n}}VF / (2RT)\right) \tag{6}$$

$$k_{34} = [\mathrm{Na}^+]_{\mathrm{o}} / \left(K_{3\mathrm{no}} + [\mathrm{Na}^+]_{\mathrm{o}}\right) \tag{7}$$

$$k_{21} = \left([\mathrm{Ca}^{2+}]_{\mathrm{o}} / K_{\mathrm{co}}\right)\exp\left(Q_{\mathrm{co}}VF / (RT)\right) / d_{\mathrm{o}} \tag{8}$$

$$k_{23} = \frac{1}{d_{\mathrm{o}}}\frac{[\mathrm{Na}^+]_{\mathrm{o}}}{K_{1\mathrm{no}}}\frac{[\mathrm{Na}^+]_{\mathrm{o}}}{K_{2\mathrm{no}}}\left(1 + \frac{[\mathrm{Na}^+]_{\mathrm{o}}}{K_{3\mathrm{no}}}\right)\exp\left(-\frac{Q_{\mathrm{n}}VF}{2RT}\right) \tag{9}$$

$$k_{32} = \exp\left(Q_{\mathrm{n}}VF / (2RT)\right) \tag{10}$$

$$x_1 = k_{34}k_{41}\left(k_{23} + k_{21}\right) + k_{21}k_{32}\left(k_{43} + k_{41}\right) \tag{11}$$

$$x_2 = k_{43}k_{32}\left(k_{14} + k_{12}\right) + k_{41}k_{12}\left(k_{34} + k_{32}\right) \tag{12}$$

$$x_3 = k_{43}k_{14}\left(k_{23} + k_{21}\right) + k_{12}k_{23}\left(k_{43} + k_{41}\right) \tag{13}$$

$$x_4 = k_{34}k_{23}\left(k_{14} + k_{12}\right) + k_{21}k_{14}\left(k_{34} + k_{32}\right) \tag{14}$$

$$I_{\mathrm{NaCa}} = k_{\mathrm{NaCa}}\left(k_{21}x_2 - k_{12}x_1\right) / \left(x_1 + x_2 + x_3 + x_4\right) \tag{15}$$

Table S11. $\boldsymbol{I_{\mathrm{p}}}$ **and** $\boldsymbol{I_{\mathrm{b}}}$.

$$I_{\mathrm{p}} = \overline{I}_{\mathrm{p}}\left(\frac{[\mathrm{Na}^+]_{\mathrm{i}}}{K_{\mathrm{m,Na}} + [\mathrm{Na}^+]_{\mathrm{i}}}\right)^3\left(\frac{[\mathrm{K}^+]_{\mathrm{o}}}{K_{\mathrm{m,K}} + [\mathrm{K}^+]_{\mathrm{o}}}\right)^2\frac{1.6}{1.5 + \exp\left(-\left(V + 60.0\right)/40.0\right)} \tag{1}$$

$$I_{\mathrm{b}} = g_{\mathrm{b}}\left(V - E_{\mathrm{b}}\right) \tag{2}$$

Table S12. Intracellular Ca^{2+}-handling.

$$j_{\mathrm{Ca,dif}} = \left([\mathrm{Ca}^{2+}]_{\mathrm{sub}} - [\mathrm{Ca}^{2+}]_{\mathrm{i}}\right) / \tau_{\mathrm{dif,Ca}} \tag{1}$$

$$j_{\mathrm{rel}} = P_{\mathrm{rel}}\left([\mathrm{Ca}^{2+}]_{\mathrm{rel}} - [\mathrm{Ca}^{2+}]_{\mathrm{sub}}\right) / \left(1 + \left(K_{\mathrm{rel}} / [\mathrm{Ca}^{2+}]_{\mathrm{sub}}\right)^2\right) \tag{2}$$

$$j_{\mathrm{up}} = P_{\mathrm{up}} / \left(1 + K_{\mathrm{up}} / [\mathrm{Ca}^{2+}]_{\mathrm{i}}\right) \tag{3}$$

$$j_{\mathrm{tr}} = \left([\mathrm{Ca}^{2+}]_{\mathrm{up}} - [\mathrm{Ca}^{2+}]_{\mathrm{rel}}\right) / \tau_{\mathrm{tr}} \tag{4}$$

$$\frac{\mathrm{d}[\mathrm{Ca}^{2+}]_{\mathrm{i}}}{\mathrm{d}t} = \frac{j_{\mathrm{Ca,dif}} V_{\mathrm{sub}} - j_{\mathrm{up}} V_{\mathrm{up}}}{V_{\mathrm{i}}} - [\mathrm{CM}]_{\mathrm{tot}} \frac{\mathrm{d}f_{\mathrm{CMi}}}{\mathrm{d}t} + [\mathrm{TC}]_{\mathrm{tot}} \frac{\mathrm{d}f_{\mathrm{TC}}}{\mathrm{d}t} + [\mathrm{TMC}]_{\mathrm{tot}} \frac{\mathrm{d}f_{\mathrm{TMC}}}{\mathrm{d}t} \tag{5}$$

$$\frac{\mathrm{d}[\mathrm{Ca}^{2+}]_{\mathrm{sub}}}{\mathrm{d}t} = \frac{1}{V_{\mathrm{sub}}}\left(\frac{-\left(I_{\mathrm{Ca,L}} - 2I_{\mathrm{NaCa}}\right)}{2F} + j_{\mathrm{rel}} V_{\mathrm{rel}}\right) - j_{\mathrm{Ca,dif}} - [\mathrm{CM}]_{\mathrm{tot}} \frac{\mathrm{d}f_{\mathrm{CMs}}}{\mathrm{d}t} - SL_{\mathrm{tot}} \frac{\mathrm{d}f_{\mathrm{CSL}}}{\mathrm{d}t} \tag{6}$$

$$\frac{\mathrm{d}[\mathrm{Ca}^{2+}]_{\mathrm{rel}}}{\mathrm{d}t} = j_{\mathrm{tr}} - j_{\mathrm{rel}} - [\mathrm{CQ}]_{\mathrm{tot}} \frac{\mathrm{d}f_{\mathrm{CQ}}}{\mathrm{d}t} \tag{7}$$

$$\frac{\mathrm{d}[\mathrm{Ca}^{2+}]_{\mathrm{up}}}{\mathrm{d}t} = j_{\mathrm{up}} - j_{\mathrm{tr}} \frac{V_{\mathrm{rel}}}{V_{\mathrm{up}}} \tag{8}$$

$$\frac{\mathrm{d}f_{\mathrm{TC}}}{\mathrm{d}t} = k_{f_{\mathrm{TC}}} [\mathrm{Ca}^{2+}]_{\mathrm{i}} \left(1 - f_{\mathrm{TC}}\right) - k_{b_{\mathrm{TC}}} f_{\mathrm{TC}} \tag{9}$$

$$\frac{\mathrm{d}f_{\mathrm{TMC}}}{\mathrm{d}t} = k_{f_{\mathrm{TMC}}} [\mathrm{Ca}^{2+}]_{\mathrm{i}} \left(1 - f_{\mathrm{TMC}} - f_{\mathrm{TMM}}\right) - k_{b_{\mathrm{TMC}}} f_{\mathrm{TMC}} \tag{10}$$

$$\frac{\mathrm{d}f_{\mathrm{TMM}}}{\mathrm{d}t} = k_{f_{\mathrm{TMM}}} [\mathrm{Mg}^{2+}]_{\mathrm{i}} \left(1 - f_{\mathrm{TMC}} - f_{\mathrm{TMM}}\right) - k_{b_{\mathrm{TMM}}} f_{\mathrm{TMM}} \tag{11}$$

$$\frac{\mathrm{d}f_{\mathrm{CMi}}}{\mathrm{d}t} = k_{f_{\mathrm{CM}}} [\mathrm{Ca}^{2+}]_{\mathrm{i}} \left(1 - f_{\mathrm{CMi}}\right) - k_{b_{\mathrm{CM}}} f_{\mathrm{CMi}} \tag{12}$$

$$\frac{\mathrm{d}f_{\mathrm{CMs}}}{\mathrm{d}t} = k_{f_{\mathrm{CM}}} [\mathrm{Ca}^{2+}]_{\mathrm{sub}} \left(1 - f_{\mathrm{CMs}}\right) - k_{b_{\mathrm{CM}}} f_{\mathrm{CMs}} \tag{13}$$

$$\frac{\mathrm{d}f_{\mathrm{CQ}}}{\mathrm{d}t} = k_{f_{\mathrm{CQ}}} [\mathrm{Ca}^{2+}]_{\mathrm{rel}} \left(1 - f_{\mathrm{CQ}}\right) - k_{b_{\mathrm{CQ}}} f_{\mathrm{CQ}} \tag{14}$$

$$\frac{\mathrm{d}f_{\mathrm{CSL}}}{\mathrm{d}t} = 115.0 \cdot 1000.0 [\mathrm{Ca}^{2+}]_{\mathrm{sub}} \left(1.0 - f_{\mathrm{CSL}}\right) - 1000.0 f_{\mathrm{CSL}} \tag{15}$$

Table S13. 1D multicellular model (SAN-AVN model as used for Figs. 3, 4 and 7).

$$C_{\mathrm{m,SAN}}(n) = 20 + 45((n-1)/24)^{1.5} \qquad (n = 1, 2, \cdots, 25) \tag{1}$$

$$C_{\mathrm{m,AM}}(n) = 50 \quad (n = 26, 27, \cdots, 100) \tag{2}$$

$$C_{\mathrm{m,FP}}(n) = \begin{cases} 50 & (n = 101, 102, \cdots, 150) \\ 40 & (n = 151, 152, \cdots, 225) \\ 29 & (n = 226, 227, \cdots, 250) \end{cases} \tag{3}$$

$$C_{\mathrm{m,SP}}(n) = \begin{cases} 50 & (n = 101, 102, \cdots, 175) \\ 29 & (n = 176, 177, \cdots, 300) \end{cases} \tag{4}$$

$$C_{\mathrm{m,NH}}(n) = \begin{cases} 29 & (n = 251, 252, \cdots, 275) \\ 40 & (n = 276, 277, \cdots, 350) \end{cases} \tag{5}$$

$$g_{\mathrm{SAN}}(n, n+1) = 25 + 975((n-1)/24)^{4} \quad (n = 1, 2, \cdots, 25) \tag{6}$$

$$g_{\mathrm{AM}}(n, n+1) = 1000 \quad (n = 26, 27, \cdots, 100) \tag{7}$$

$$g_{\mathrm{FP}}(n, n+1) = \begin{cases} 1000 - \dfrac{500}{1.0 + \exp((n-125.5)/-5.0)} & (n = 101, 102, \cdots, 150) \\ 500 & (n = 151, 152, \cdots, 225) \\ 300 & (n = 226, 227, \cdots, 250) \end{cases} \tag{8}$$

$$g_{\mathrm{SP}}(n, n+1) = \begin{cases} 1000 - \dfrac{700}{1.0 + \exp((n-138)/-5.0)} & (n = 101, 102, \cdots, 175) \\ 500 & (n = 176, 177, \cdots, 300) \end{cases} \tag{9}$$

$$g_{\mathrm{NH}}(n, n+1) = \begin{cases} 300 & (n = 251, 251, \cdots, 275) \\ 500 & (n = 276, 277, \cdots, 349) \end{cases} \tag{10}$$

$$g_{\mathrm{Na,SAN}}(n) = (6.07 \times 10^{2})(C_{\mathrm{m,SAN}}(n) - 20.0)/45.0 \qquad (n = 1, 2, \cdots, 25) \tag{11}$$

$$g_{\mathrm{Na,AM}}(n) = 7.09 \times 10^{2} \quad (n = 26, 27, \cdots, 100) \tag{12}$$

$$g_{\mathrm{Na,FP}}(n) = \begin{cases} 7.09 \times 10^{2} & (n = 101, 102, \cdots, 150) \\ 2.53 \times 10^{2} & (n = 151, 152, \cdots, 225) \\ \dfrac{2.53 \times 10^{2}}{1 + \exp((n-238)/2.5)} & (n = 226, 227, \cdots, 250) \end{cases} \tag{13}$$

$$g_{\mathrm{Na,SP}}(n) = \begin{cases} 7.09 \times 10^{2} & (n = 101, 102, \cdots, 175) \\ 0.00 & (n = 176, 177, \cdots, 300) \end{cases} \tag{14}$$

$$g_{\mathrm{Na,NH}}(n) = \begin{cases} \dfrac{2.53\times 10^{2}}{1+\exp((n-263)/-2.5)} & (n = 251, 252, \cdots, 275) \\ 2.53\times 10^{2} & (n = 276, 277, \cdots, 350) \end{cases} \tag{15}$$

Table S14. 1D multicellular model (AVN model as used for Figs. 2, 5, 6, 8 and 9).

$$C_{\mathrm{m,AM}}(n) = 50 \quad (n = 1, 2, \cdots, 50) \tag{1}$$

$$C_{\mathrm{m,FP}}(n) = \begin{cases} 50 & (n = 51, 52, \cdots, 100) \\ 40 & (n = 101, 102, \cdots, 150) \\ 29 & (n = 151, 152, \cdots, 175) \end{cases} \tag{2}$$

$$C_{\mathrm{m,SP}}(n) = \begin{cases} 50 & (n = 50, 51, \cdots, 125) \\ 29 & (n = 126, 127, \cdots, 200) \end{cases} \tag{3}$$

$$C_{\mathrm{m,NH}}(n) = \begin{cases} 29 & (n = 176, 177, \cdots, 200) \\ 40 & (n = 201, 202, \cdots, 250) \end{cases} \tag{4}$$

$$g_{\mathrm{AM}}(n, n+1) = 1000 \quad (n = 1, 2, \cdots, 50) \tag{5}$$

$$g_{\mathrm{FP}}(n, n+1) = \begin{cases} 1000 - \dfrac{500}{1.0 + \exp((n - 75.5)/-5.0)} & (n = 51, 52, \cdots, 100) \\ 500 & (n = 101, 102, \cdots, 175) \end{cases} \tag{6}$$

$$g_{\mathrm{SP}}(n, n+1) = \begin{cases} 1000 - \dfrac{500}{1.0 + \exp((n - 88)/-5.0)} & (n = 51, 52, \cdots, 125) \\ 500 & (n = 126, 127, \cdots, 199) \end{cases} \tag{7}$$

$$g_{\mathrm{NH}}(n, n+1) = 500 \quad (n = 176, 177, \cdots, 249) \tag{8}$$

$$g_{\mathrm{Na,AM}}(n) = 7.09 \times 10^2 \quad (n = 1, 2, \cdots, 50) \tag{9}$$

$$g_{\mathrm{Na,FP}}(n) = \begin{cases} 7.09 \times 10^2 & (n = 51, 52, \cdots, 100) \\ 2.53 \times 10^2 & (n = 101, 102, \cdots, 150) \\ \dfrac{2.53 \times 10^2}{1 + \exp((n - 163)/2.5)} & (n = 151, 152, \cdots, 175) \end{cases} \tag{10}$$

$$g_{\mathrm{Na,SP}}(n) = \begin{cases} 7.09 \times 10^2 & (n = 51, 52, \cdots, 125) \\ 0.00 & (n = 126, 127, \cdots, 200) \end{cases} \tag{11}$$

$$g_{\mathrm{Na,NH}}(n) = \begin{cases} \dfrac{2.53 \times 10^2}{1 + \exp((n - 188)/-2.5)} & (n = 176, 177, \cdots, 200) \\ 2.53 \times 10^2 & (n = 201, 202, \cdots, 250) \end{cases} \tag{12}$$

Table S15. Constants for the AN, N and NH cell models.

	AN	N	NH
C_m (pF)	40.0	29.0	40.0
g_{Na} (nS)	2.53×10^2	0.00	2.53×10^2
$g_{Ca,L}$ (nS)	18.5	9.0	21.0
$E_{Ca,L}$ (mV)	62.1	62.1	62.1
g_{to} (nS)	20.0	0.00	14.0
$g_{K,r}$ (nS)	1.50	3.50	2.00
g_f (nS)	0.00	1.00	0.00
g_{st} (nS)	0.00	0.100	0.00
$g_{K,1}$ (nS)	12.5	0.00	15.0
g_b (nS)	1.80	1.20	2.00
E_b (mV)	−52.5	−22.5	−40.0
k_{NaCa} (nA)	5.92	2.14	5.92
$I_{p,max}$ (pA)	24.6	1.43×10^2	1.97×10^2
$[Na^+]_o$ (mM)	1.40×10^2	1.40×10^2	1.40×10^2
$[Ca^{2+}]_o$ (mM)	2.00	2.00	2.00
$[K^+]_o$ (mM)	5.40	5.40	5.40
$[Na^+]_i$ (mM)	8.00	8.00	8.00
$[K^+]_i$ (mM)	1.40×10^2	1.40×10^2	1.40×10^2

Table S16. Starting values for the AN, N and NH cell models.

	AN	N	NH
V (mV)	−70.03	−62.13	−68.63
m	0.01227	–	0.01529
h_1	0.7170	–	0.6438
h_2	0.6162	–	0.5552
d_L	4.069×10^{-5}	1.533×10^{-4}	5.025×10^{-5}
$f_{L,fast}$	0.9985	0.6861	0.9981
$f_{L,slow}$	0.9875	0.4441	0.9831
$p_{a,fast}$	0.07107	0.6067	0.09949
$p_{a,slow}$	0.04840	0.1287	0.07024
p_i	0.9866	0.9775	0.9853
q	8.857×10^{-3}	–	9.581×10^{-3}
r_{fast}	0.8734	–	0.8640
r_{slow}	0.1503	–	0.1297
y	–	0.03825	–
q_a	–	0.1933	–
q_i	–	0.4886	–
$[Ca^{2+}]_i$ (μM)	0.1206	0.3623	0.1386
$[Ca^{2+}]_{sub}$ (μM)	0.06397	0.2294	0.07314
$[Ca^{2+}]_{rel}$ (mM)	0.4273	0.08227	0.4438
$[Ca^{2+}]_{up}$ (mM)	1.068	1.146	1.187
f_{TC}	0.02359	0.6838	0.02703
f_{TMC}	0.3667	0.6192	0.4020
f_{TMM}	0.5594	0.3363	0.5282
f_{CMi}	0.04845	0.1336	0.05530
f_{CMs}	0.02626	0.08894	0.02992
f_{CQ}	0.3379	0.08736	0.3463
f_{CSL}	3.936×10^{-5}	4.764×10^{-5}	4.843×10^{-5}

Table S17. Constants for the atrial cell model.

	Original	Modified
C_{m} (pF)	50.0	50.0
P_{Na} (pl/s)	1.40×10^{3}	1.40
g_{Na} (nS)	708.5×10^{3}	708.5
$g_{\mathrm{Ca,L}}$ (nS)	4.00	4.00
$g_{\mathrm{Ca,T}}$ (nS)	6.00	6.00
g_{to} (nS)	50.0	35.0
$g_{\mathrm{K,r}}$ (nS)	3.50	7.00
$g_{\mathrm{K,s}}$ (nS)	2.50	5.00
$g_{\mathrm{K,1}}$ (nS)	5.09	10.0
$[\mathrm{Na}^{+}]_{\mathrm{o}}$ (mM)	1.40×10^{2}	1.40×10^{2}
$[\mathrm{Ca}^{2+}]_{\mathrm{o}}$ (mM)	2.50	2.50
$[\mathrm{K}^{+}]_{\mathrm{o}}$ (mM)	5.00	5.00

Table S18. Starting values for the atrial cell model.

V (mV)	-80.96
m	3.012×10^{-3}
h_1	0.9764
h_2	0.8861
d_L	5.440×10^{-3}
f_L	1.000
d_T	7.473×10^{-3}
f_T	0.6052
r	8.217×10^{-6}
s_1	0.8624
s_2	0.3943
s_3	0.6071
p_a	3.533×10^{-5}
p_i	0.5898
n	7.838×10^{-3}
$[Na^+]_i$ (mM)	8.438
$[K^+]_i$ (mM)	139.88
$[Ca^{2+}]_i$ (mM)	0.05538
$[Ca^{2+}]_{up}$ (mM)	0.5077
$[Ca^{2+}]_{rel}$ (mM)	0.4561
O_c	0.02396
O_{TnCa}	0.01156
O_{TnMgMg}	0.2055
O_{Calse}	0.3534
F_1	0.2535
F_2	1.183×10^{-3}
F_3	0.6482

Fig. S1

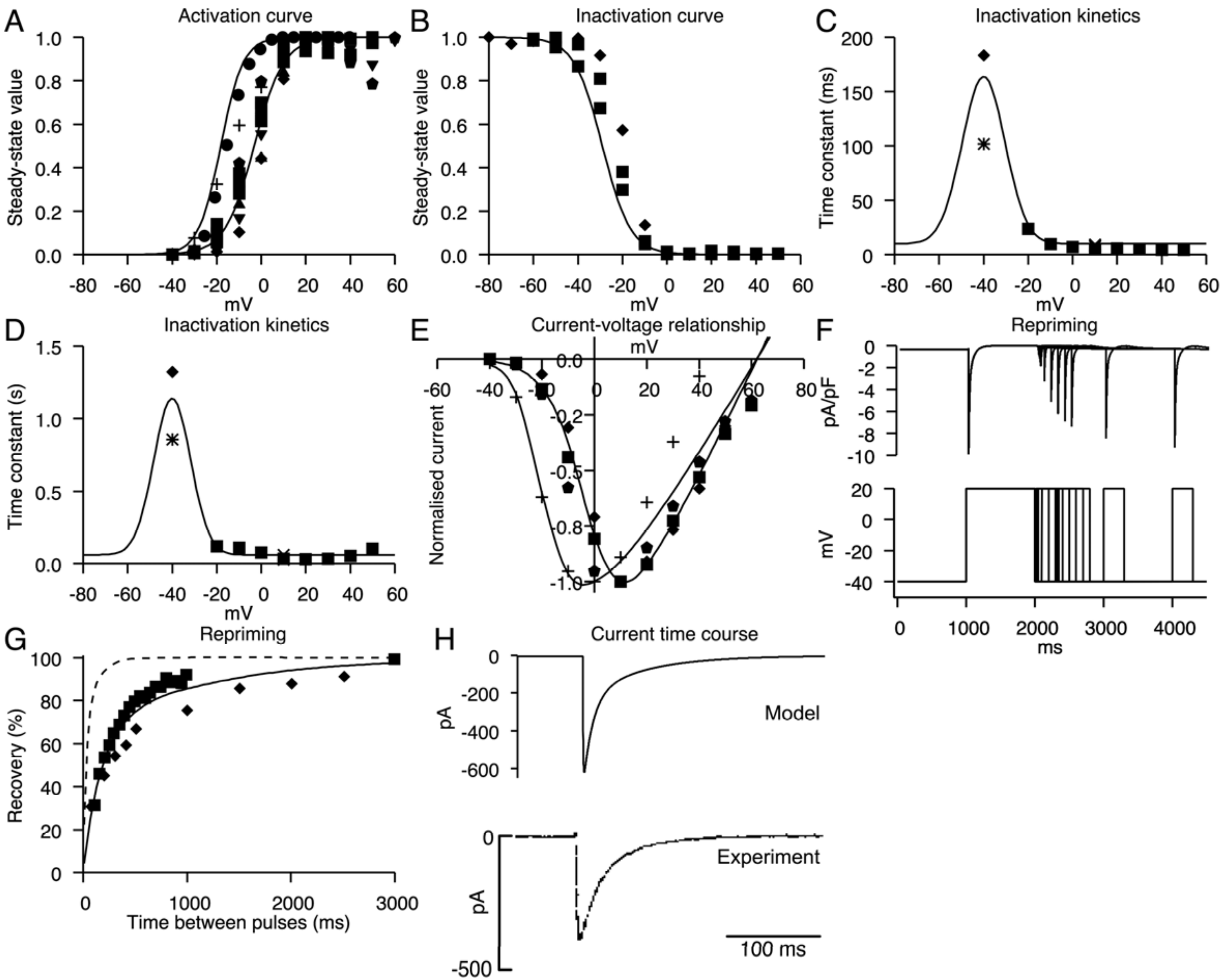
A
Activation curve
Steady-state value
mV
B
Inactivation curve
Steady-state value
mV
C
Inactivation kinetics
Time constant (ms)
mV
D
Inactivation kinetics
Time constant (s)
mV
E
Current-voltage relationship
mV
Normalised current
F
Repriming
pA/pF
mV
ms
G
Repriming
Recovery (%)
Time between pulses (ms)
H
Current time course
pA
Model
pA
Experiment
100 ms

Fig. S2

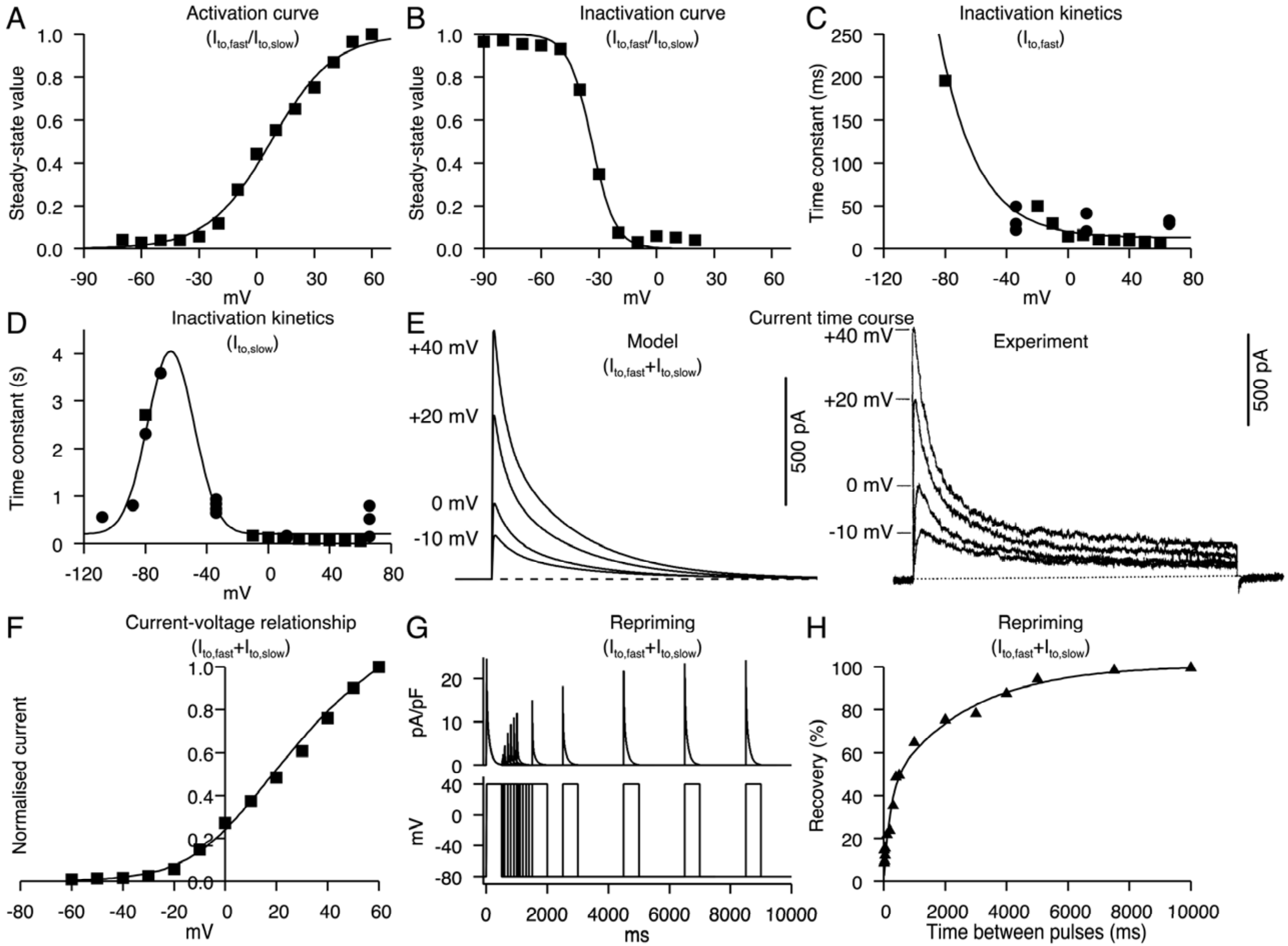

A
Activation curve
($I_{to,fast}/I_{to,slow}$)
Steady-state value
mV
B
Inactivation curve
($I_{to,fast}/I_{to,slow}$)
Steady-state value
mV
C
Inactivation kinetics
($I_{to,fast}$)
Time constant (ms)
mV
D
Inactivation kinetics
($I_{to,slow}$)
Time constant (s)
mV
E
Current time course
Model
($I_{to,fast}+I_{to,slow}$)
+40 mV
+20 mV
0 mV
-10 mV
500 pA
Experiment
+40 mV
+20 mV
0 mV
-10 mV
500 pA
F
Current-voltage relationship
($I_{to,fast}+I_{to,slow}$)
Normalised current
mV
G
Repriming
($I_{to,fast}+I_{to,slow}$)
pA/pF
mV
ms
H
Repriming
($I_{to,fast}+I_{to,slow}$)
Recovery (%)
Time between pulses (ms)

Fig. S3

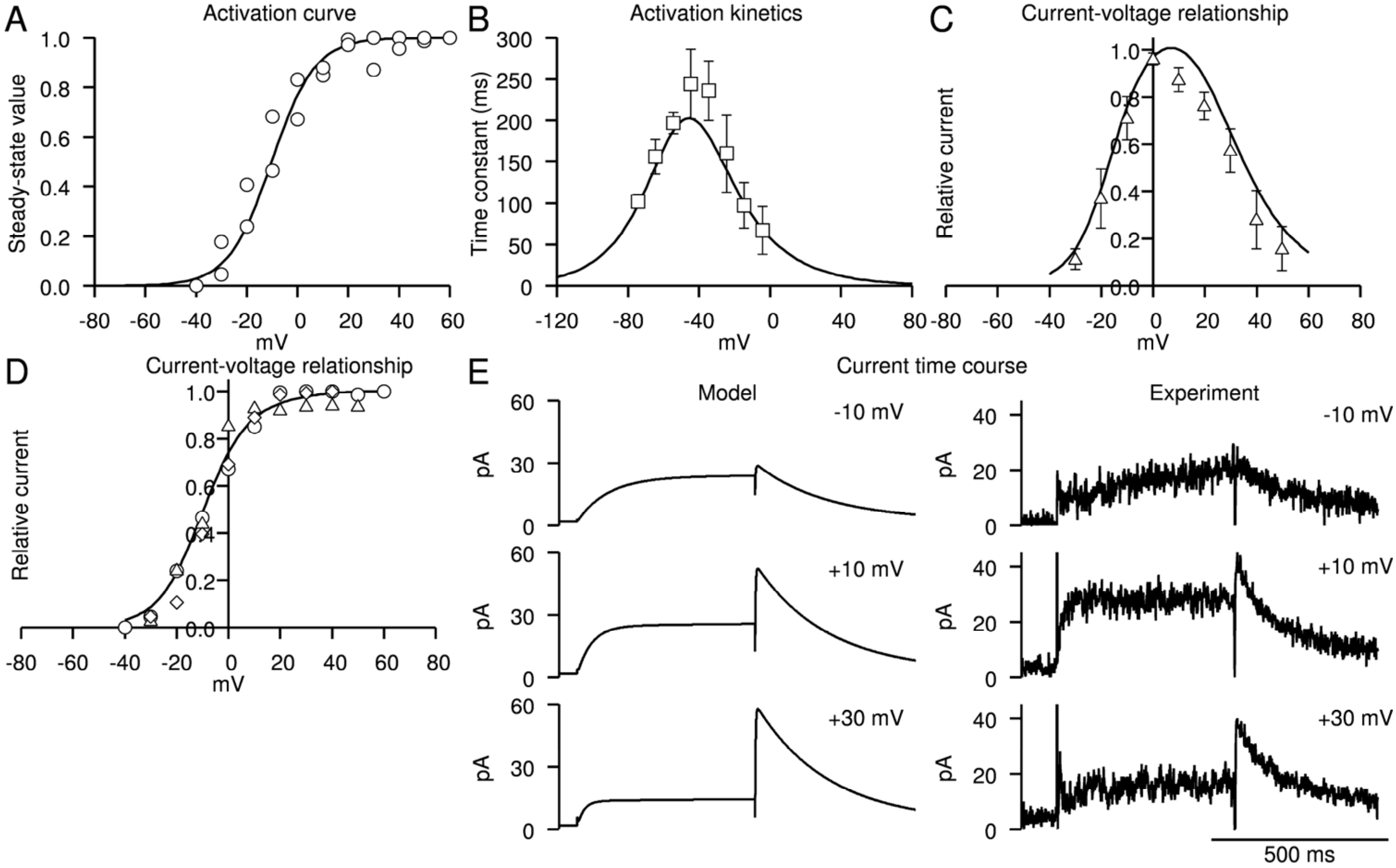
A
Activation curve
Steady-state value
mV
B
Activation kinetics
Time constant (ms)
mV
C
Current-voltage relationship
Relative current
mV
D
Current-voltage relationship
Relative current
mV
E
Current time course
Model
Experiment
pA
-10 mV
+10 mV
+30 mV
500 ms

Fig. S4

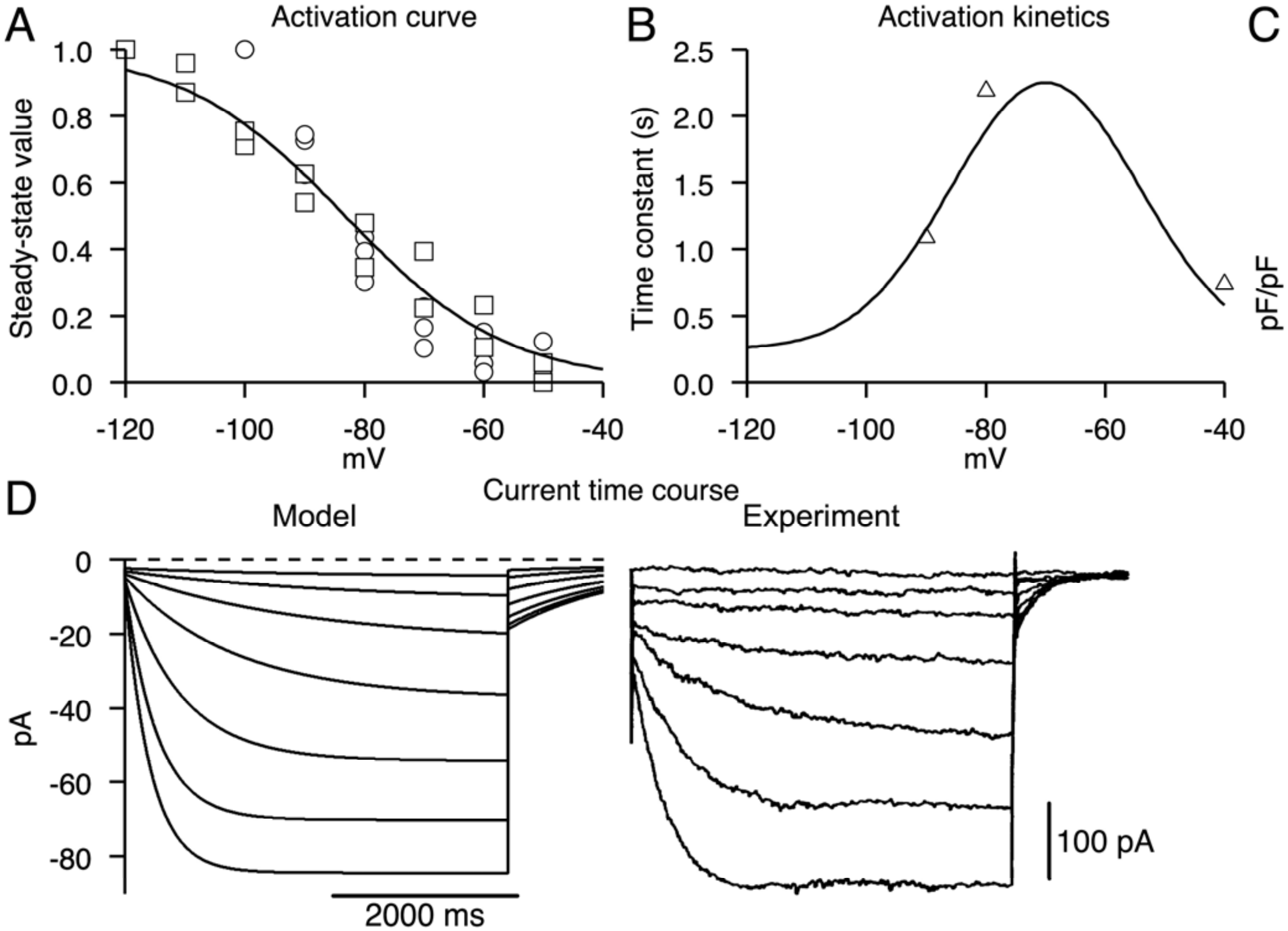
A
Activation curve
Steady-state value
1.0
0.8
0.6
0.4
0.2
0.0
-120
-100
-80
-60
-40
mV
B
Activation kinetics
Time constant (s)
2.5
2.0
1.5
1.0
0.5
0.0
-120
-100
-80
-60
-40
mV
C
Current-voltage relationship
mV
-120 -110 -100 -90 -80 -70 -60 -50
0
-1
-2
-3
pF/pF
D
Current time course
Model
Experiment
0
-20
-40
-60
-80
pA
2000 ms
100 pA

Fig. S5

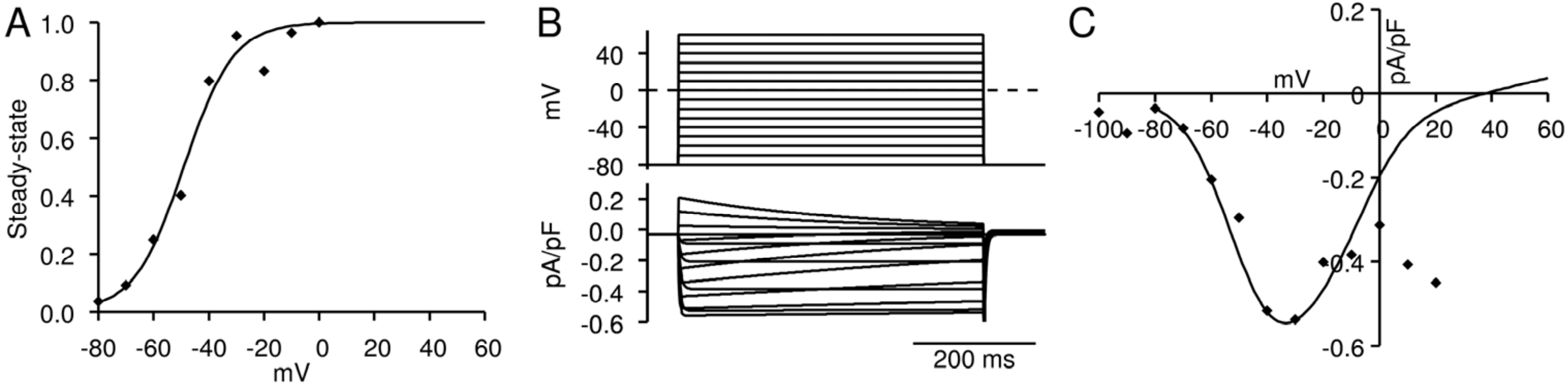
A
1.0
0.8
0.6
0.4
0.2
0.0
Steady-state
-80 -60 -40 -20 0 20 40 60
mV
B
40
0
-40
-80
mV
0.2
0.0
-0.2
-0.4
-0.6
pA/pF
200 ms
C
0.2
pA/pF
mV
0
-100 -80 -60 -40 -20 0 20 40 60
-0.2
-0.4
-0.6

Fig. S6

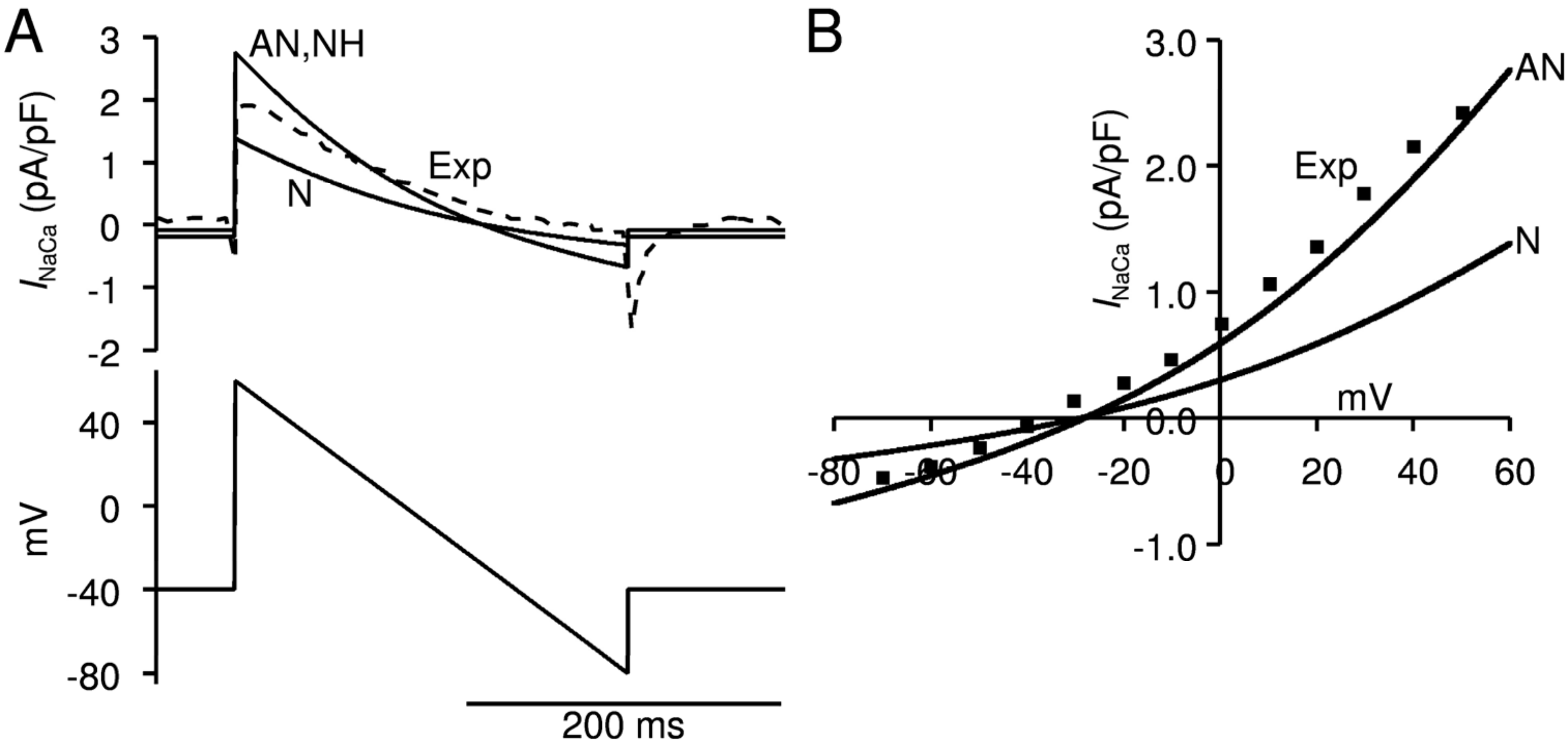
A
3
2
1
0
-1
-2
AN,NH
Exp
N
I_{NaCa} (pA/pF)
40
0
-40
-80
mV
200 ms
B
3.0
2.0
1.0
0.0
-1.0
AN
Exp
N
I_{NaCa} (pA/pF)
mV
-80
-60
-40
-20
0
20
40
60

Fig. S7